JOURNAL OF SOLID STATE CHEMISTRY **137,** 148–160 (1998)
ARTICLE NO. SC987744

Negative Thermal Expansion in $Sc_2(WO_4)_3$

J. S. O. Evans,[1] T. A. Mary, and A. W. Sleight[2]

Department of Chemistry and Center for Advanced Materials Research, Oregon State University, Corvallis, OR 97331-4003

Received September 18, 1997, in revised form December 24, 1997; accepted January 1, 1998

$Sc_2(WO_4)_3$ has been found to show the highly unusual property of negative thermal expansion over a temperature range of 10 to 1073 K. Powder neutron diffraction data from 10 to 450 K shows an essentially linear decrease in cell volume as a function of temperature. The intrinsic linear coefficient of thermal expansion from this data is $-2.2\times10^{-6}\,K^{-1}$. The linear coefficient of thermal expansion measured on a ceramic bar of $Sc_2(WO_4)_3$ can be as negative as $-11\times10^{-6}\,K^{-1}$ due to microstructure changes as a function of temperature. Rietveld refinement as a function of temperature suggests that the intrinsic negative thermal expansion can be related to transverse vibrations of bridging oxygen atoms in the structure. The anharmonic nature of these vibrations leads to a coupled tilting of the quasi-rigid framework polyhedra. This tilting in turn causes the structure to become more dense with increasing temperature.

INTRODUCTION

The majority of known materials have a positive coefficient of thermal expansion; that is, they expand on heating. We have been interested in materials which show the opposite effect, contracting with increasing temperature (1). Recent work has described negative thermal expansion in a variety of cubic systems (2–5). Such materials have potential applications both as pure phases and as components of composite materials with overall coefficients of thermal expansion adjusted to a desired value, which can include zero thermal expansion. Applications range from the high-tech to the more mundane and include electronic components, printed circuit boards, optical substrates, low temperature thermocouples, catalyst supports, and cookware. Recently, we have discovered unusual thermal expansion in a large class of molybdates and tungstates of the type $A_2(MO_4)_3$, where A is an octahedral cation and M is Mo^{6+} or W^{6+} (6, 7). In this paper, we report on the detailed structure as a function of temperature of one member of this family, $Sc_2(WO_4)_3$. The room temperature structure of this compound has been previously reported by Abrahams and Bernstein (8). We also present a mechanism for the unusual negative thermal expansion, which likely applies to other materials in this family as well.

[1]Current address: Dept. Chemistry, University of Durham, UK.
[2]To whom correspondence should be addressed.

EXPERIMENTAL

Single phase samples of $Sc_2(WO_4)_3$ were prepared by standard solid state techniques from the constituent oxides by repeated grinding and firing at 1100°C in a platinum crucible.

Neutron diffraction data were collected on the high resolution powder diffractometer at beam line H1A of the high flux beam reactor (HFBR) at Brookhaven National Laboratory with a wavelength of 1.8857 Å. Fuller details of the experimental setup have been described elsewhere (9, 10). The multibank detector was moved in 0.05° steps, with integration times of 5 minutes per step. Spectra were recorded at 10, 50, 100, 150, 200, 250, 300, 350, 400, and 450 K using a two-stage Air Products displex. Data at 150 K contained rogue points due to an individual detector bank failure, and were not used for detailed Rietveld refinement.

All structure refinements and calculations were performed with the GSAS suite of programs (11). Further details are given in the relevant part of the main text. Due to space considerations only selected fractional atomic coordinates and distances and angles are presented. Full details of each refinement model at each temperature have been deposited, and are available on request.

A Netzsch thermal analysis system was used to obtain dilatometer data. Fused silica was used for the internal components of the dilatometer. A sapphire standard was used for calibration purposes.

STRUCTURE REFINEMENT

The structure of $Sc_2(WO_4)_3$ was refined in space group *Pnca* at nine temperatures between 10 and 450 K using the atomic positions of Abrahams and Bernstein (8) as a starting model. Since we were interested in the very minor changes in bond distances and angles that occur as a function of temperature, care was taken to adopt a consistent refinement strategy at each temperature. For each of the refinements

0022-4596/98 $25.00

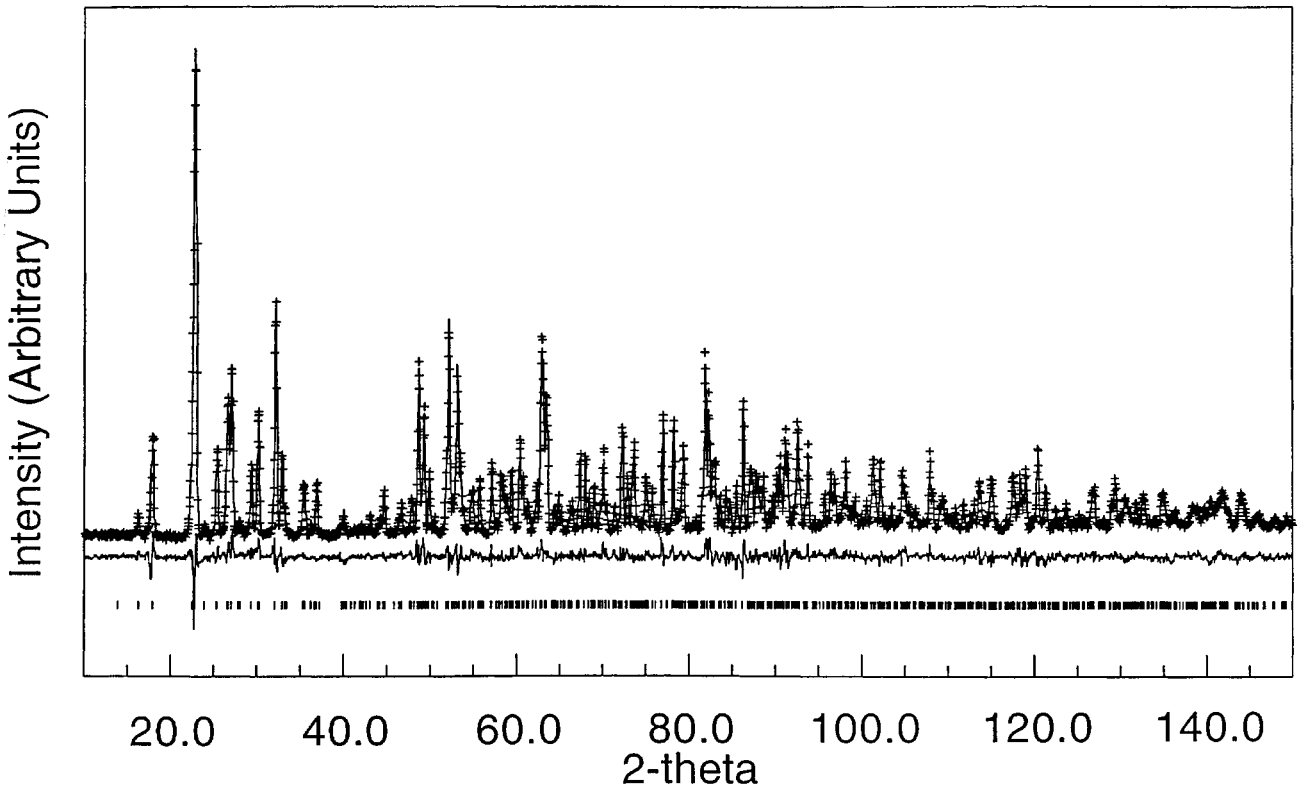

FIG. 1. Observed (+), calculated (line), and difference (lower line) neutron diffraction patterns for free isotropic model of refinement (see text) of $Sc_2(WO_4)_3$ at 300 K. Lower tick marks represent predicted peak positions.

discussed below, in addition to the fractional atomic coordinates and thermal parameters, the following parameters were refined: 12 background variables, 3 profile variables, 3 cell parameters, zero point, and an overall scale factor: a total of 20 "histogram variables." Figure 1 shows observed, calculated, and difference profiles of a typical refinement.

Figure 2 and Table 1 show the temperature dependence of the *a*, *b*, and *c* cell parameters and the overall unit cell volume as a function of temperature. The values reported are based on a model in which peak shape asymmetry was not refined; this gives the most accurate cell dimensions possible in the absence of an internal standard. An essentially linear contraction of *a* (-6.3×10^{-5} Å K^{-1}) and *c* (-5.5×10^{-5} Å K^{-1}) and an expansion of *b* ($+7.5\times10^{-5}$ Å K^{-1}) are observed over the entire temperature range. A small leveling of the curves is seen between 10 and 50 K; expansion coefficients are therefore quoted from linear regression of the 50 to 450 K data points. Figure 2b shows that the relative magnitudes of the cell edge changes are sufficient to give an overall contraction in the total cell volume, and thus a negative thermal expansion. The overall volume contraction is well represented by $V = 1236.4 - 0.008\times T$ Å^3, corresponding to $\alpha_V = -6.5\times10^{-6}$ K^{-1}, using the simple assumption that $\alpha_l = 1/3\alpha_V$ gives $\alpha_1 = -2.2\times10^{-6}$ K^{-1}.

The overall changes in bond distances and angles as a function of temperature in this and other negative thermal expansion materials are small. In addition, it is well known that apparent changes in bond distances as a function of temperature can occur due to correlated thermal vibrations (vide infra). In order to investigate these effects and minimize the influence of such correlations on the structural interpretation, a number of different refinement strategies were investigated. The differences between these individual strategies will be discussed in turn, though we emphasize at the outset that despite minor differences in detail, each model provides essentially the same indication as to the source of negative thermal expansion in these materials.

Isotropic free atom refinement. Initial refinement was performed using an isotropic thermal parameter for each atom (34 atomic, 55 total parameters). Excellent agreement was attained at each temperature; weighted profile R-factors (*wRp* values) ranging from 8.05 to 7.69% for the nine temperatures (average value 7.82%); overall χ^2 for all nine refinements 2.422. Fractional atomic coordinates at representative temperatures of 10, 300, and 450 K are shown in

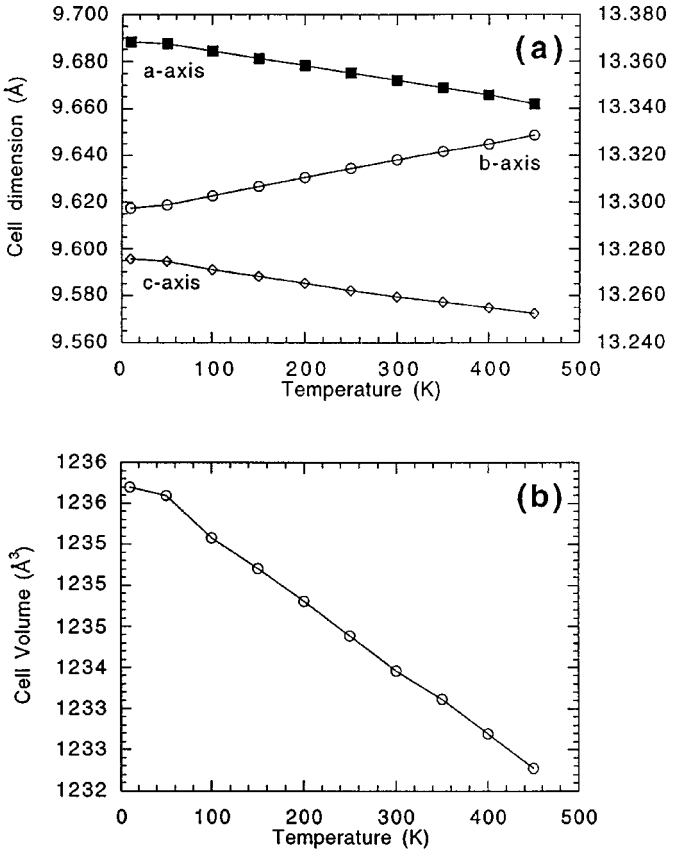

FIG. 2. (a) Unit cell parameters vs temperature. (b) Cell volume vs temperature.

Table 2. Complete sets of fractional atomic coordinates and bond distances for each refinement have been deposited, and are available on request. Bond distances and angles at 300 K are shown in Table 3.

Examination of octahedral and tetrahedral bond angles of the ScO_6 and WO_4 polyhedra that make up the framework structure revealed only small distortions from ideal geometry. Octahedral angles ranged from 88.0° (O2–Sc–O4 at 250 K) to 93.2° (O3–Sc–O6, 10 K). Examination of individual bond angles also indicated minimal distortions as a function of temperature. The maximum angular variation of an individual ScO_6 90° bond angle over the entire temperature range was 0.85°; the average variation was 0.53°.[3] These variations can be compared to a typical Rietveld standard deviation on the measured angle of 0.18°–0.25°.

WO_4 tetrahedral bond angles ranged from 107.9° (O3–W2–O5, 400 K) to 111.7° (O3–W2–O6, 450 K), with a slightly larger spread of values with temperature. The maximum variation was 1.7° (O2–W1–O4) though the average angular variation was again only 0.87° (typical standard deviations of individual angles: 0.3°–0.6°).

[3]Angular variation is defined here as the difference between the maximum and minimum value found for an individual bond angle over the whole temperature range; average angular variation is the average of these values for the 12 individual ScO_6 90° angles.

TABLE 1
Cell Dimensions as a Function of Temperature

Temperature (K)	*a* (Å)	*b* (Å)	*c* (Å)	Vol (Å^3)	w*R*p (%)	*R*(F^2) (%)
10.00	9.6883	13.297	9.5956	1236.2	8.05	4.93
50.00	9.6875	13.299	9.5947	1236.1	7.85	4.93
100.00	9.6843	13.303	9.5911	1235.6	7.72	4.90
150.00	9.6812	13.307	9.5881	1235.2		
200.00	9.6784	13.310	9.5852	1234.8	7.57	5.35
250.00	9.6753	13.314	9.5822	1234.4	7.69	5.57
300.00	9.6720	13.318	9.5795	1234.0	7.19	5.68
350.00	9.6689	13.322	9.5773	1233.6	7.42	5.93
400.00	9.6659	13.325	9.5749	1233.2	7.54	6.29
450.00	9.6620	13.329	9.5725	1232.8	7.54	6.89

Note: Rietveld esd's of 0.0002 Å (*a* and *c*) and 0.0003 Å (*b*) at each temperature are an underestimate of the absolute precision of the measurement. w*R*p and *R*(F^2) values from a rigid body (WO_4) model of refinement are also quoted.

Scandium oxygen bond distances again revealed only minor deviations from octahedral symmetry, ranging from 2.075 (Sc–O3, 400 K) to 2.118 Å (Sc–O6, 10 K). Individual bond distances varied little with temperature, the maximum variation of an individual bond length being 0.017 Å, the average variation 0.013 Å (esd of typical distance: 0.006 Å). The overall average Sc–O distance remained essentially unchanged as a function of temperature, varying from 2.0973 Å at 10 K to 2.0960 Å at 450 K [d_{av}(Sc–O) = 2.0973 $- 2.88 \times 10^{-6}$T Å].

Tungsten oxygen bond distances showed a similarly small departure from ideality, ranging from 1.733 Å (W2–O6, 400 K) to 1.773 Å (W2–O5, 10 K) with a maximum variation of 0.022 Å and average variation of 0.016 Å. The overall average W–O bond distance, however, showed a slight apparent decrease as a function of temperature from 1.7604 Å (10 K) to 1.7511 Å (450 K) [d_{av}(W–O) = 1.7606 $- 2.12 \times 10^{-5}$T Å]. This apparent thermal contraction is, however, almost certainly caused by coupled thermal vibrations of the W–O bonds, as discussed below, and bond shrinkage is not the true cause of negative thermal expansion in this material.

Individual thermal parameters for each atom increased smoothly as a function of temperature, again suggesting a reliable model with no significant systematic errors at any individual temperature. Average oxygen isotropic temperature factors are well represented by the equation $u_{iso} = 0.0041 + 4.5 \times 10^{-5}$T Å^2 (R = 99.95%), all individual values lying within 0.003 Å^2 of this line (A small departure from linearity was perhaps evident at 10 K as expected on a simple Einstein model; owing to the low number of

TABLE 2
Fractional Atomic Coordinates at 10, 300, and 450 K[a]

Name	*X*	*Y*	*Z*	$u^*_{iso}100$
		10 K		
Sc1	0.46534(21)	0.38045(15)	0.24894(28)	1.01(5)
W1	0.250000	0.000000	0.4751(7)	0.55(18)
W2	0.1191(5)	0.35551(35)	0.3969(5)	− 0.25(11)
O1	0.0926(4)	0.14109(32)	0.0781(4)	0.40(11)
O2	0.1267(4)	0.06006(29)	0.3692(4)	0.33(11)
O3	0.0127(4)	0.26289(32)	0.3233(4)	0.57(10)
O4	0.3318(4)	0.40929(30)	0.0810(4)	0.77(10)
O5	0.0759(4)	0.47350(31)	0.3229(4)	0.47(10)
O6	0.2923(5)	0.32959(28)	0.3638(4)	0.61(10)
		300 K		
Sc1	0.46688(22)	0.38110(17)	0.24937(31)	1.33(5)
W1	0.250000	0.000000	0.4743(8)	1.29(22)
W2	0.1188(6)	0.3557(4)	0.3949(5)	0.68(14)
O1	0.0917(5)	0.14199(39)	0.0770(5)	1.73(13)
O2	0.1302(5)	0.06284(35)	0.3693(5)	2.09(14)
O3	0.0118(5)	0.26323(38)	0.3215(5)	2.00(13)
O4	0.3358(5)	0.41072(34)	0.0787(5)	1.81(13)
O5	0.0733(5)	0.47255(36)	0.3226(5)	1.71(13)
O6	0.2923(5)	0.33169(35)	0.3608(5)	1.64(12)
		450 K		
Sc1	0.46740(23)	0.38146(18)	0.24892(34)	1.58(5)
W1	0.250000	0.000000	0.4744(9)	1.54(23)
W2	0.1179(6)	0.3555(4)	0.3941(6)	0.91(15)
O1	0.0916(5)	0.1422(4)	0.0750(5)	2.36(15)
O2	0.1323(6)	0.0636(4)	0.3689(6)	2.78(15)
O3	0.0119(6)	0.2623(4)	0.3209(6)	2.72(15)
O4	0.3373(6)	0.4119(4)	0.0779(6)	2.76(16)
O5	0.0699(5)	0.4720(4)	0.3228(6)	2.51(15)
O6	0.2917(6)	0.3335(4)	0.3598(5)	2.17(13)

[a]Refinement based on free isotropic model (see text).

TABLE 3
Selected Bond Distances (Å) and Angles (deg) at 300 K

	O1	O2	O3	O4	O5	O6
Sc1	2.079(5)	2.086(5)	2.086(5)	2.109(5)	2.109(5)	2.105(5)
W1		1.749(6)		1.763(6)		
W2	1.765(7)		1.757(7)		1.760(7)	1.740(7)
Sc1–O–W	151.7(3)	171.0(3)	154.2(4)	148.3(3)	174.4(3)	144.3(3)

low-temperature data points, parameterization of this dependency was not attempted). Metal temperature factors are: Sc, $u_{iso} = 0.0088 + 1.3 \times 10^{-5}T$ (R = 98.7%); W1, $u_{iso} = 0.0056 + 3.36 \times 10^{-5}T$ (R = 97%); W2, $u_{iso} = -0.0023 + 2.18 \times 10^{-5}T$ (R = 94%), where the figure in parentheses represents the quality of fit of a straight line to the observed data. Below 100 K the W2 temperature factor becomes very slightly negative.

The apparent thermal parameters of all atoms in the structure continue to decrease in an essentially linear fashion to at least 10 K. The fact that little leveling off is observed, as would be expected for a harmonic oscillator as it approached its zero point energy, suggests that $kT \gg h\nu$ at all temperatures studied, i.e., even down to the lowest temperatures, some low frequency vibrational modes remain active. It is presumably these modes which are responsible for the continued thermal expansion down to low temperatures. We note also that "thermal parameters" or "temperature factors" can often take into account effects such as atomic disorder and are more correctly termed "atomic displacement factors" (12). Since there is no evidence to suggest atomic disorder, and a linear decrease in these parameters is observed as the temperature is reduced over the entire temperature range studied, we choose to retain the term thermal parameters for the discussions of this paper.

Analysis of Sc–O–W bond angles and Sc–W nonbonded distances as a function of temperature did show significant and smooth variations, suggesting a model for the negative thermal expansion in this material. These results were essentially identical to those obtained using rigid body refinement and will be discussed in more detail below.

Rigid body refinement. It is well established that the thermal vibrations of individual atoms of many strongly bonded groups are highly correlated (13–15). Such groups are referred to as rigid bodies. It is apparent from free isotropic refinement that the assumption of rigid ScO_6 and WO_4 tetrahedra in $Sc_2(WO_4)_3$ is a good one. The oscillations of these polyhedra can then be described using the TLS method of Schomaker and Trueblood, whereby the overall thermal motion is described by the components of the individual translation, libration and screw tensors (16–18). The full treatment involves a total of 20 variables (6T, 6L, and 8S) to describe thermal motion, and thus for any general rigid body containing more than 3 atoms represents a reduction in the number of refined parameters. Clearly though there is an inherent assumption in such a model that internal vibrations of the "rigid" body are relatively unimportant.

The correlated oscillations of such a group can lead to apparent decreases in bond distance as a function of temperature (Fig. 3). Examples of this phenomenon are diverse, and include C–C bond lengths in benzene, O–H bond lengths in layered metal hydroxides, and Si–O bond lengths in silicate materials (14, 19, 20). This effect can be taken into account by a post-refinement bond length correction as originally described by Cruickshank (21).

Free isotropic refinement suggests that the individual polyhedra within the $Sc_2(WO_4)_3$ structure remain essentially undistorted as a function of temperature. Rigid body refinement was therefore attempted based on two extreme

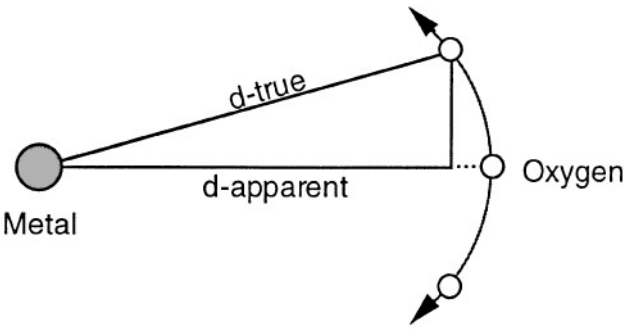

FIG. 3. The effect of correlated thermal motion on apparent bond lengths.

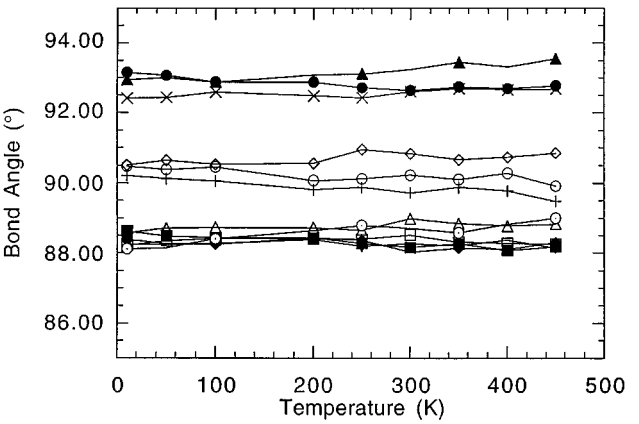

FIG. 4. ScO_6 90° internal bond angles as a function of temperature for the rigid WO_4 model. Typical esd's are 0.25° for ScO_6 angles. Individual angles are O1–Sc–O3, open circles; O1–Sc1–O5, open squares; O1–Sc1–O6, open diamonds; O2–Sc1–O1, crosses; O2–Sc1–O3, upright lines, O2–Sc1–O5, open triangles; O3–Sc1–O6, solid circles; O4–Sc1–O2, solid squares, O4–Sc1–O5, solid diamonds; O4–Sc1–O3, solid triangles pointing up; O4–Sc1–O6, solid triangles pointing down; and O5–Sc1–O6, open circles with point.

assumptions (the true picture presumably lying between these two extremes): rigid octahedral ScO_6 groups or rigid tetrahedral WO_4 groups.

Rigid bodies were defined using the 10 K data set, where vibrational effects are presumably minimized, and a single overall temperature factor. Average bond distances of 2.0944 Å for ScO_6, 1.7637 Å for $W1O_4$, and 1.7579 Å for $W2O_4$ resulted. In treating the thermal motion of the rigid bodies we make several assumptions. Firstly, we assume that all elements of the S tensor are zero. Thus correlations between translational and librational motion are ignored, which is equivalent to assuming that the origin of the rigid body is also its origin of vibration. Secondly, only a single diagonal term was refined for both T and L tensors (i.e., $t_{11} = t_{22} = t_{33}$; $l_{11} = l_{22} = l_{33}$; all other terms are zero) this constrains the overall $u_{\text{equivalent}}$ values of each oxygen to be identical.

Refinement using this protocol and a rigid ScO_6 octahedron (14 atomic variables) led to an average wRp over all temperatures of 7.74%, and positive temperature factors for all refinements. It is important to emphasize that this model of rigid body refinement led to a reduction in the average R-factor from 7.82 to 7.74% relative to free isotropic refinement, despite a reduction in the number of refined atomic parameters from 34 to 14.

Refinement based on rigid WO_4 groups and anisotropic Sc thermal parameters required 21 atomic variables and gave wRp values ranging from 8.05% (at 10 K) to 7.19% (at 300 K) [average = 7.62%], and an overall χ^2 value of 2.287. Temperature factors for all atoms remained positive definite over the entire temperature range. This model did, however, lead to a slight apparent reduction in the average Sc–O distance from 2.0970 Å at 10 K to 2.0847 Å at 450 K [$d_{av}(Sc–O) = 2.0978 - 2.75 \times 10^{-5}T$], due to the correlated motions discussed above. Equally, refinement based on rigid ScO_6 groups leads to a slight reduction in the W–O bond length from 1.7623 Å (10 K) to 1.7516 Å (450 K) [$d_{av}(W–O) = 1.7625 - 2.419 \times 10^{-5}T$]. Crystallochemical consideration of the bonds in the structure would suggest that the true situation for this compound would be that the W–O bonds would remain essentially unchanged as a function of temperature, whereas one might expect a slight increase in the Sc–O bond length (22, 23). In addition, the average O–O distance within a WO_4 tetrahedron is slightly less than for a ScO_6 octahedron [$d_{av}(O–O) = 2.875$ Å for WO_4; $d_{av}(O–O) = 2.962$ Å for ScO_6], suggesting greater rigidity for a WO_4 group. Since both extreme rigid body models gave essentially identical variations in the bridging bond angles and polyhedral tilts of interest in determining the thermal expansion behavior of these materials, we choose to concentrate on the rigid WO_4-based refinement for the rest of this paper.

Figure 4 shows the temperature dependence of the unconstrained O–Sc–O internal polyhedral bond angles as a function of temperature. Only minor deviations in these bond angles are observed, supporting our rigid body assumption. The temperature dependence of the structurally most significant changes in bond distances and angles is shown graphically in Figs. 7 and 8. Full sets of atomic coordinates and complete tables of distances and angles for each of the various refinement models at each temperature have been deposited, and are available from the authors on request.

THERMAL EXPANSION BY DIRECT MEASUREMENT

The thermal expansion of $Sc_2(WO_4)_3$ was also measured on sintered ceramic bars with approximate dimensions of

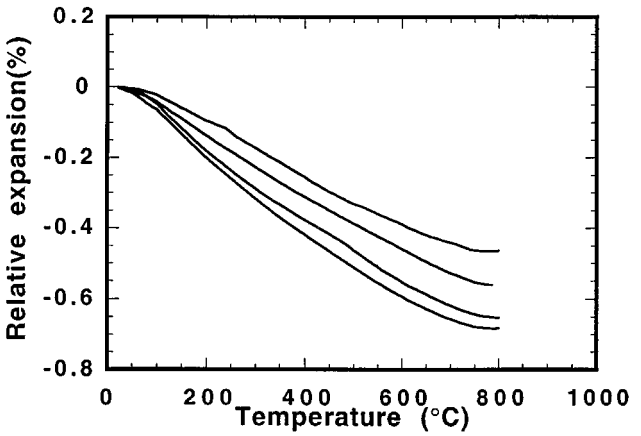

FIG. 5. Thermal expansion data for $Sc_2(WO_4)_3$ based on dilatometer data on several different ceramic bars.

$5 \times 5 \times 25$ mm. Typical thermal expansion behavior of such bars is shown in Fig. 5. These results suggest that the thermal expansion of $Sc_2(WO_4)_3$ may remain negative up to its congruent melting point of 1640°C (24). Thermal expansion of ceramic bars of $Sc_2(WO_4)_3$ measured by dilatometry ranged from $-6 \times 10^{-6}\,K^{-1}$ to $-11 \times 10^{-6}\,K^{-1}$. The latter value is apparently a new record for the highest magnitude negative thermal expansion over an extended temperature range. These values are much more negative than the $-2.2 \times 10^{-6}\,K^{-1}$ value derived from unit cell edges with temperature. This difference can be related to microcracking (25). When crystallites in a ceramic body are expanding in some directions but contracting in other directions, microcracks are formed on cooling from the temperature at which the ceramic was consolidated. These cracks enlarge on cooling and tend to disappear again on heating. The result is negative thermal expansion of an extrinsic type. The very negative thermal expansion of $-11 \times 10^{-6}\,K^{-1}$ in $Sc(WO_4)_3$ is due then to a combination of the intrinsic $-2.2 \times 10^{-6}\,K^{-1}$ thermal expansion with the extrinsic effect of microcracking. In isotropic materials such as ZrW_2O_8, ZrP_2O_7, and ZrV_2O_7, we have always found good agreement between dilatometry and diffraction results (2–5).

Dilatometer measurements have been reported on a single crystal of $Sc_2(WO_4)_3$ (26). These results should agree with our diffraction results, but they do not. Values of α for *a*, *b*, and *c* were reported to be -5.45, $+5.60$, and $+4.43 \times 10^{-6}\,K^{-1}$, whereas we find -6.5, -1.60, and $-5.73 \times 10^{-6}\,K^{-1}$. A different choice of axes cannot explain this discrepancy, because we calculate a linear thermal expansion coefficient of $-2.2 \times 10^{-6}\,K^{-1}$, whereas their results give a linear thermal expansion coefficient of $-0.87 \times 10^{-6}\,K^{-1}$. We have measured the axial thermal expansion coefficients of several tungstates and molybdates of the $A_2(MO_4)_3$ family. The values are consistently negative for *a* and *c* but positive for *b* (6, 7).

DISCUSSION

The structure of $Sc_2(WO_4)_3$ consists of a corner sharing network of ScO_6 octahedra and WO_4 tetrahedra. There is a single Sc site (8d) in the asymmetric unit and two crystallographically distinct W atoms, one (W1) on the twofold axis (4c) and the other (W2) on a general position (8d). Each ScO_6 octahedron corner shares with six WO_4 tetrahedra; each WO_4 corner shares with four ScO_6 octahedra. This results in a relatively open framework structure (the shortest Sc–Sc distance at 300 K is 5.26 Å) of metal atoms linked by two coordinate oxygens.

The overall three-dimensional framework structure can perhaps be best understood by breaking it down into 2D slabs of corner sharing polyhedra parallel to the *ac* plane, which stack together to form the overall structure. Each individual slab can be considered as being formed by the cross-linking (via O1 and O2) of "lantern like" $(ScO_6)_2(WO_4)_3$ groups (Fig. 6). This arrangement leaves a single oxygen (O3) to join individual slabs parallel to the *b* axis. This two-dimensional viewpoint of the structure frequently reveals itself in a high degree of preferred orientation in powder patterns of materials with this structure (27).

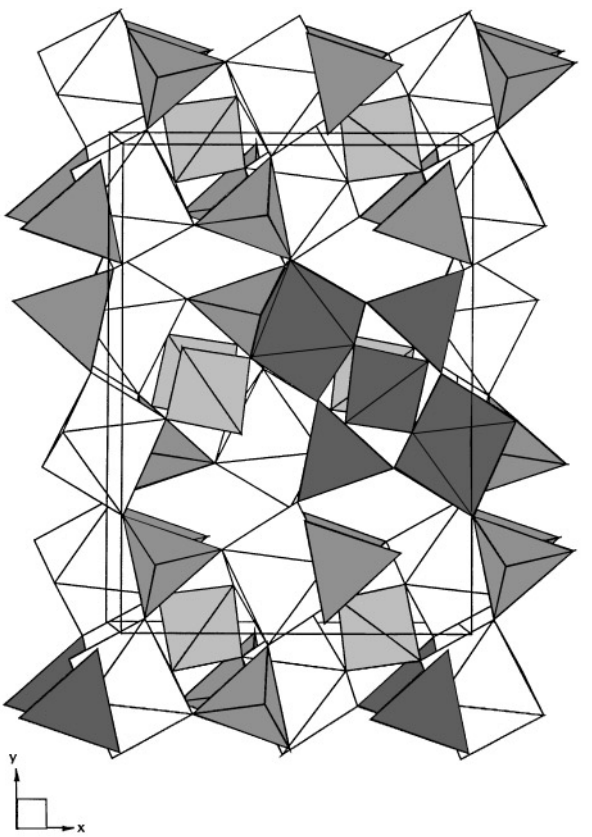

FIG. 6. Polyhedral representation of the structure of $Sc_2(WO_4)_3$. ScO_6 octahedra in white, $W1O_4$ tetrahedra in light gray, $W2O_4$ tetrahedra in darker gray. A $(ScO_6)_2(WO_4)_3$ "lantern" group is highlighted.

The individual Sc–O–W bridging bond angles vary from 144.1° (Sc–O6–W2) to 174.2° (Sc–O5–W2); this in turn leads to a range of Sc–W nonbonded distances from 3.670 to 3.863 Å. The temperature dependence of these bridging angles and the resultant changes in the corresponding Sc–W distances are shown graphically in Fig. 7. It can be seen from this figure that significant changes occur in these angles as the temperature is increased. This, coupled with the relatively small variations in internal polyhedral bond distances and angles, suggests that the structural changes occurring can be described as being due to the coupled rotation of essentially rigid polyhedra.

Figure 8 shows the tilt angles of the three different polyhedra in the structure as a function of temperature. Here we have chosen to arbitrarily define the tilt angle relative to three Cartesian axes (x, y, z parallel to a, b, c) of the rigid WO_4 groups at 10 K as 0°. Tilt angles shown correspond to the angles of rotation around each Cartesian axis in turn required to superimpose the low temperature polyhedron on the high. Tilt angles of the ScO_6 group (not directly determined by the Rietveld analysis) were derived by a least squares fit of the 10 K ScO_6 group to the refined (and therefore potentially slightly distorted) coordinates at a given temperature. Gratifyingly, tilt angles derived in this manner differed from those derived from refinement using a ScO_6 rigid body by less than 0.1°. Figure 9 shows projections down the three crystallographic axes of the low and high temperature ScO_6 octahedra. The magnitudes of the individual tilts have been scaled up five times for clarity. Figure 10 shows how the projected bond angles vary as a function of temperature.

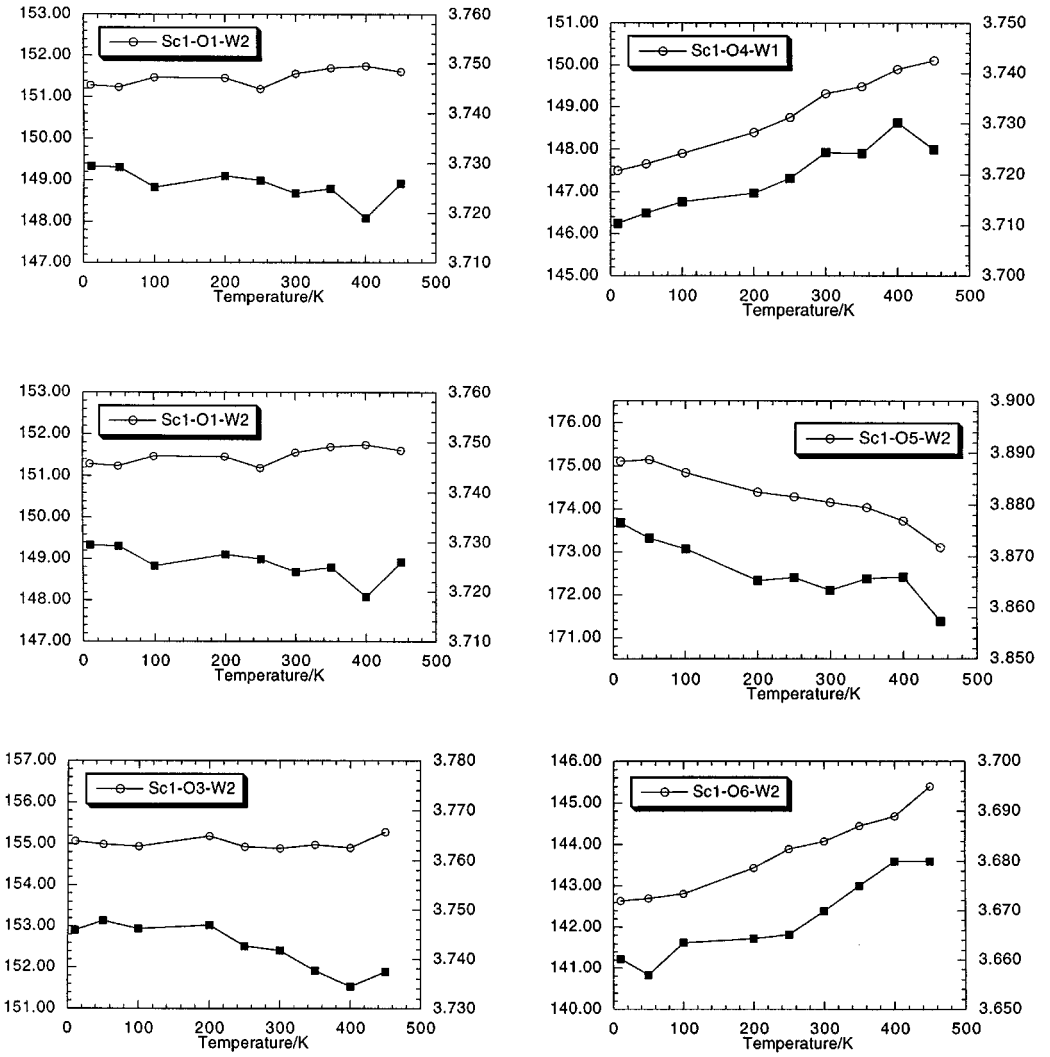

FIG. 7. Sc–O–W bond angles (open points) and corresponding Sc–W nonbonded distances (closed points) as a function of temperature for rigid WO_4 model. All graphs plotted over a 6°/0.05 Å range; esd angle 0.20°, distance 0.004 Å.

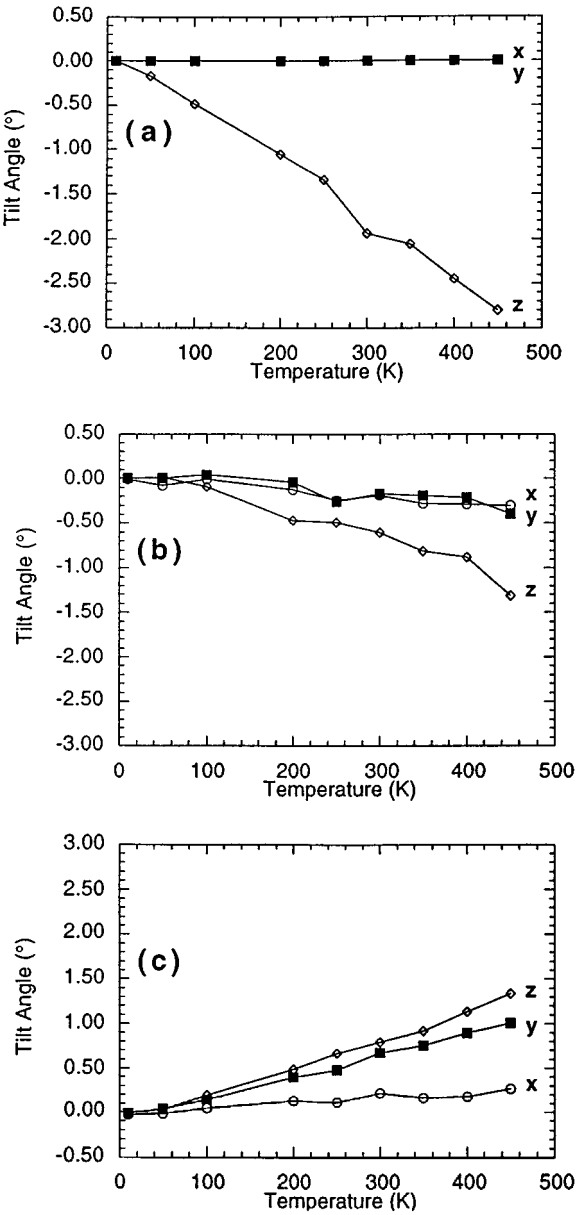

FIG. 8. Magnitude of polyhedral tilts around x, y, and z axes (parallel to a, b, and c, respectively). Typical esd 0.2°. (a) $W1O_4$; (b) $W2O_4$; (c) ScO_6.

Due to the complexity of the vertex sharing arrangement of the constituent polyhedra of the $Sc_2(WO_4)_3$ lattice, the variety of different bridging bond angles present, and the slight distortions of the individual polyhedra from ideality, the coupling of different polyhedral tilts is complicated. A rigorous mathematical analysis of the dependence of cell parameters and individual atomic coordinates on tilt angles, as can be performed for less complex structures such as quartz (18), is beyond the scope of this paper. Considerable insight can, however, be gained by less quantitative considerations. Firstly, we consider the origin of the polyhedral tilting in this lattice.

In the solid state atoms are not stationary, but undergo continual oscillations. Atomic coordinates derived from diffraction measurements represent the mean atomic positions. In the case of a framework lattice made up of semirigid polyhedral building blocks some vibrational modes or, if one restricts oneself to a localized view, some oscillations of the constituent polyhedra will be of lower energy than others. These low energy modes will be most significantly populated at a given temperature and will therefore give rise to the largest atomic displacements. If the restoring potential for a given mode is asymmetric, an anharmonic thermal vibration results, and a net displacement of atomic positions as a function of temperature is observed. Such a process is shown schematically in Fig. 11.

For framework lattices the lowest energy modes are generally those involving a transverse vibration of the 2-coordinate bridging oxygen groups, which tend to leave metal–oxygen bond lengths unchanged. Simple considerations show that if such a mode leads to an overall decrease in the M–O–M′ bridging angle, the M–M′ distance will on average decrease, and a negative coefficient of thermal expansion will result. Consideration of Fig. 9a and the individual bond angle changes of Fig. 7 shows that an isolated z-axis tilt of a rigid ScO_6 group in which the direction of the Sc–W vector remained unchanged would lead to a decrease (giving a negative contribution to the coefficient of thermal expansion) of bond angles 5, 2, 1, and 3 and an increase in angles 4 and 6. Similarly a positive y axis tilt would suggest a decrease in angles 4 and 2, yet an increase in 1, 3, 5, and 6. The actual picture is, however, complicated by the effects of the combination of three sequential tilts and the small displacements of W1 and W2 coordinates which occur on tilting. Figure 10 attempts to simplify the overall picture by plotting the sum of the projection of the individual bridging bond angles on to each plane of Fig. 9. A marked overall decrease in the total bridging bond angles for the two major tilt axes (y and z) is seen.

The driving force for polyhedral tilting in this lattice can then be ascribed to the fact that the lowest energy vibrational modes tend to cause an overall decrease in M–O–M′ bond angles. This appears to be a general phenomenon for framework lattices comprised of covalently bonded MO_n polyhedra linked by 2-coordinate oxygen, provided the network adopts its highest symmetry state.

The powder diffraction data allows us to examine further the link between polyhedral tilt angles and thermal librations. From the experimentally refined TLS matrix it is possible to derive rms libration angles for the individual polyhedra as a function of temperature. Figure 11b shows both the change in rms libration of $W1O_4$ and the polyhedral tilt angle as a function of temperature. Since $W1O_4$ lies on a twofold axis, only a single tilt angle need be considered. It can be seen that there is good correlation between the tilt angle and the change in rms libration as a function of

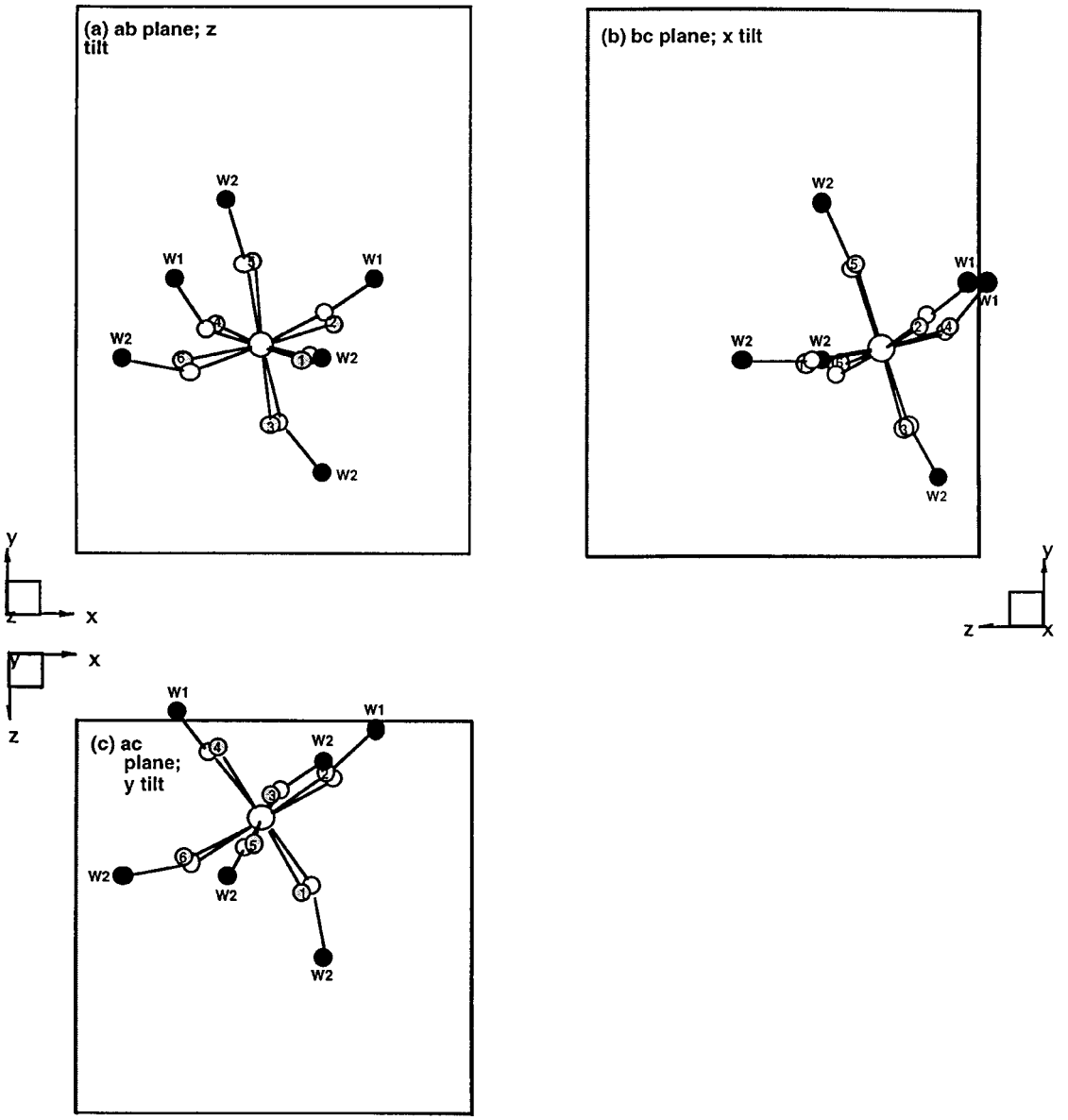

FIG. 9. Projections of the ScO_6 octahedron viewed down (a) the *c* axis [*ab* plane]; (b) the *a* axis [*bc* plane]; and (c) the *b* axis [*ac* plane]. Low temperature oxygen positions shown as small open circles, high temperature positions as numbered circles. High temperature W positions have been omitted. Polyhedral tilts have been magnified 5 times relative to their 450 K values for clarity.

temperature. Linear regression yields a change in tilt angle of $0.0064^\circ\,K^{-1}$, and a change in rms libration of $0.0062^\circ\,K^{-1}$. This suggests an interpretation similar to that of Fig. 11a, whereby an asymmetric change in rms libration angle of 3° results in an apparent 3° tilt of the polyhedron.

If one makes the simplifying assumption that the most important forces determining the volume of a unit cell of a framework lattice are due to first neighbor attractive interactions and next nearest neighbor repulsive interactions, then it follows that at the lowest temperatures the volume of any framework structure will be maximized. This is since the attractive component of the structure remains fixed by the fixed metal–oxygen distance, whilst the repulsive component can be minimized by adopting the maximum volume possible without expanding M–O distances. In the simple case of a ReO_3^- like framework, this would give rise to 180° M–O–M bridging bond angles; in more complex framework topologies 180° angles may not be achievable. Since we are concentrating on modes which tend to leave M–O bond distances unchanged, it follows that as repulsive interactions have already maximized the cell volume, all such modes can only lead to a decrease in the

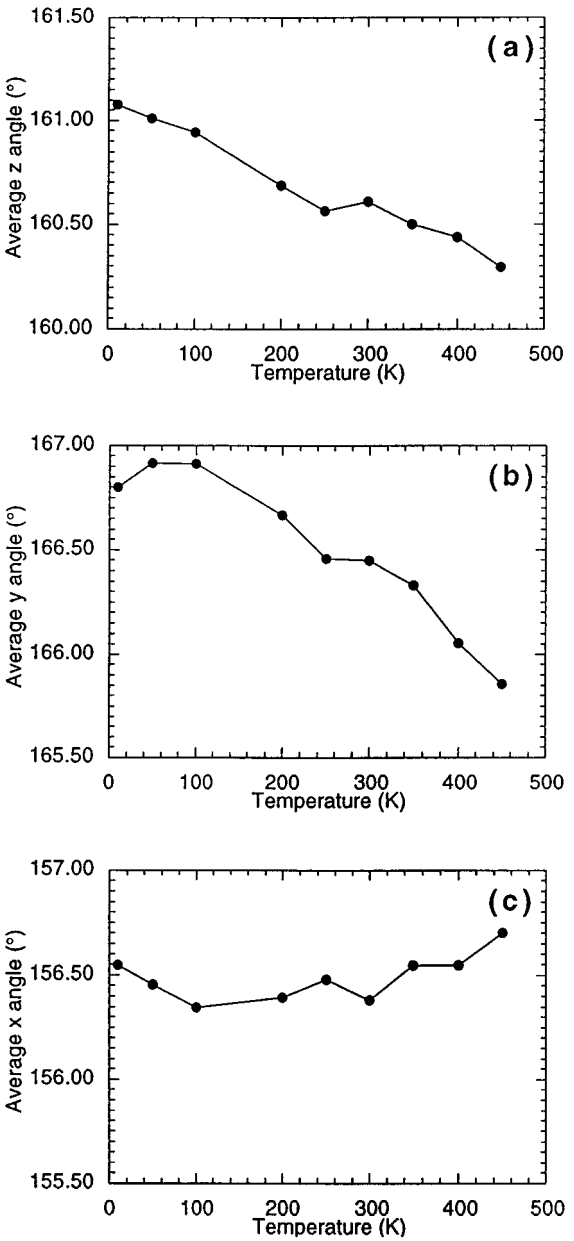

FIG. 10. Projected bond angles as a function of temperature. Average bond angles projected onto (a) the *ab*, (b) the *ac*, and (c) the *bc* planes.

average M–O–M′ bond angle and hence a decrease in the cell volume. Similar considerations also explain the phenomenon that many framework lattices (e.g., ZrV_2O_7, ZrP_2O_7, SiO_2, $Sc_2(MoO_4)_3$, $In_2(WO_4)_3$, etc.) only show negative thermal expansion in their high symmetry states. The low temperature displacive phase transitions in such structures must be caused by longer range forces than those considered above. These long range interactions lead to a stabilization of the structure, and cause a reduction in the cell volume. As the volume is no longer maximized, low energy modes may be present which tend to expand the lattice. The displacive phase transition to the high symmetry structure can be considered to occur when the displacement of a bridging atom due to its thermal motion becomes equal to its displacement from the ideal high symmetry site. At this point long range ordering forces have effectively been destroyed by thermal energy, and the lattice again adopts its maximum volume.[4] Beyond this temperature, however, the only remaining low energy modes are again those which tend to contract the lattice, and negative thermal expansion ensues.

The sign and magnitudes of thermal expansion coefficients along the three axes of the unit cell can be best understood by considering the $W1O_4$ tetrahedron as the fixed pivot point around which all polyhedral tilts occur. Such a view is convenient since only the *z*-coordinate of W1 is free to move and one need consider only a *z*-axis tilt. As discussed above, the $Sc_2(WO_4)_3$ structure can be considered as being built up from the cross-linking along the *b* axis of corner sharing polyhedral slabs in the *ac* plane. The only linkage between these slabs is via O3. Figure 7 shows that this angle undergoes no significant change as a function of temperature. We therefore restrict our discussion of the overall changes in cell dimensions to changes within the two-dimensional slabs. Figure 12 show views down the three crystallographic axes of a representative portion of a single slab. These views correspond to those of Fig. 9; the scandium atom of Fig. 9 has been asterisked for clarity. Discussion will concentrate on this Sc and its two adjoining W1 atoms. At 10 K, the plane of O1, O2, O4, and O6 (hereafter the *xy* octahedral plane) is inclined at a small angle to the *ac* plane. As the temperature is increased, W1 tilts in an anticlockwise manner around the twofold axis (parallel to *c*). Scandium octahedra bond to W1 via both O2 and O4. The anticlockwise rotation of O2 (which links octahedron 1 with the right-hand $W1O_4$ group of Fig. 12a) tends to bring the *xy* plane of the octahedron closer to the *ac* plane of the unit cell. Conversely, the anticlockwise rotation of O4 tends to increase this angle. However, since the relative distance Sc–O2–W1 is greater than Sc–O4–W1 both in three dimensions (Fig. 7) and in projection (Fig. 9a), and the decrease in the bond angle Sc–O2–W1 ($-4.4°$) is greater than the increase in Sc–O4–W1 ($+1.3°$), the net result is that the *xy* plane of each ScO_6 octahedron becomes more closely aligned to the *ac* plane of the unit cell. As

[4]This description is, of course, an oversimplification of a true solid in that it concentrates on a single mode of the lattice. In a real system other modes will of course become populated as the temperature is raised, modes which themselves will tend to expand or contract the lattice. For this reason, the cell volume at the phase transition need not necessarily correspond to the maximum volume expected based on geometrical considerations.

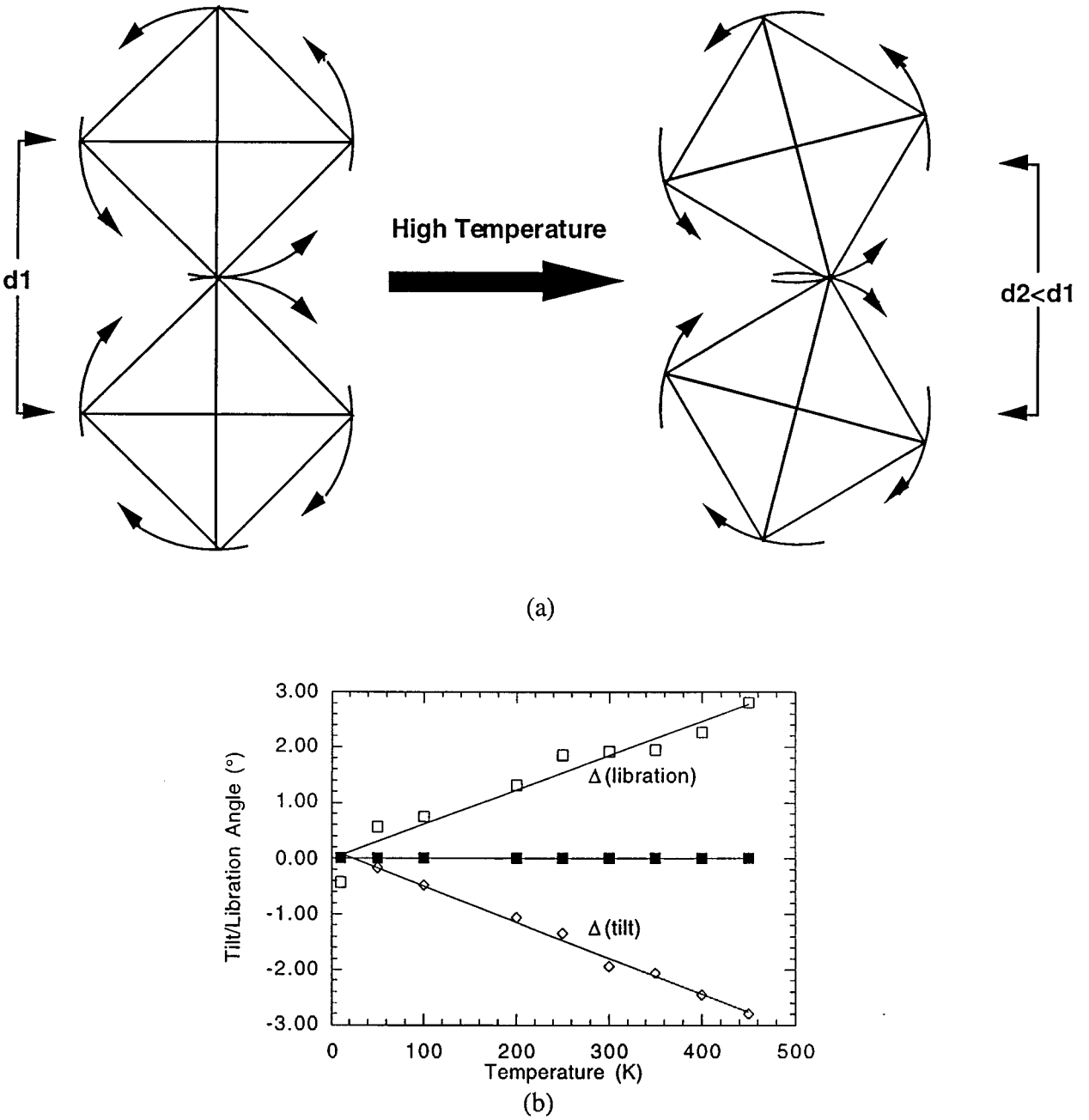

FIG. 11. (a) A schematic representation of how an anharmonic thermal vibration can lead to tilting of polyhedral groups. On the left is represented a hypothetical low temperature structure. As the temperature is raised, anharmonic thermal vibration occurs, the magnitude of which is represented by the curved arrows. Mean atomic positions at high temperature are at the center of the anharmonic oscillations; this leads to an overall increase in polyhedral tilting as a function of temperature and a decrease in the centroid–centroid or metal-metal distance. (b) Correlation between experimentally determined libration angles and static tilt angles for $W1O_4$.

a consequence, the octahedral z axis (i.e., Sc–O5) becomes more closely aligned to the b axis of the unit cell. This results in an expansion of the slab in the b direction and an overall increase in the b axis as a function of temperature.

The same $W1O_4$ rotation also causes a shift of the ScO_6 octahedra parallel to the a axis. (Fig. 12a). Using essentially the same arguments as above, two Sc atoms move farther apart in the a direction (Fig. 12a, numbers 3 and 4), while two move closer together (1 and 2). Again the relative magnitude of the two effects leads to an overall contraction of the a axis. Over the temperature range studied, Sc1 and Sc2 of Fig. 12 move closer together in the a direction by

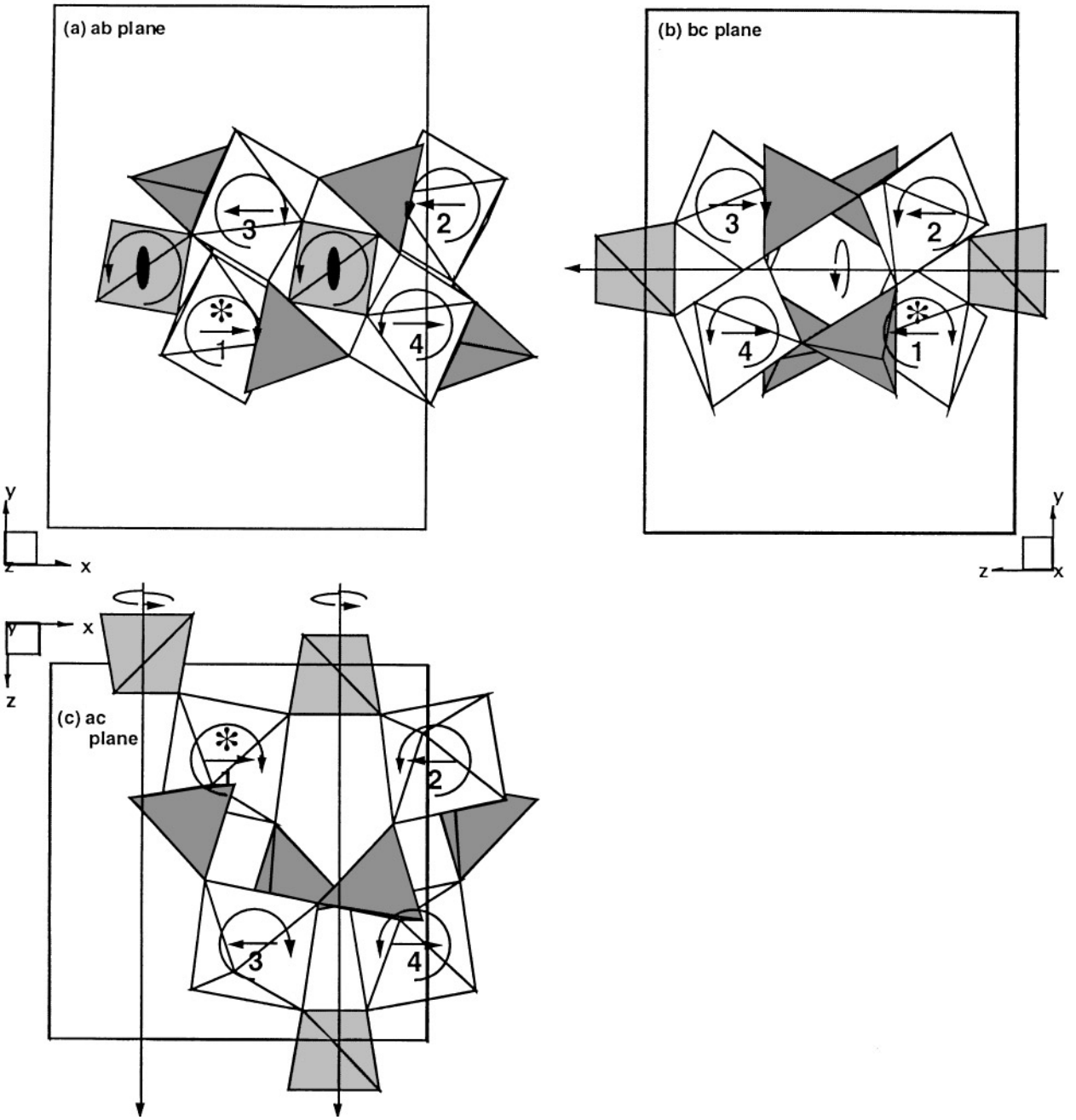

FIG. 12. The direction of polyhedral tilts in the $Sc_2(WO_4)_3$ lattice. Views correspond to those of Fig. 9. The Sc atom of Fig. 9 is marked * (Sc1). Sc 2, 3, and 4 octahedra are related to Sc1 by symmetry. $W1O_4$ octahedra on the twofold axis are shaded light gray, $W2O_4$ dark gray. The twofold symmetry axis is emphasized in each figure.

0.051 Å while Sc3 and Sc4 move farther apart by 0.026 Å, giving an overall effective contraction. Such a picture is somewhat of an oversimplification in that the same rotation actually brings Sc1/4 and Sc2/3 slightly closer together along the *b* direction. However, the magnitudes of the accompanying polyhedral tilts are such that the overall slab thickness as defined by the O3–O3′ distance along the *b* axis increases steadily as a function of temperature. Finally, Fig. 12b shows schematically the effect on the *c* axis of bringing the ScO_6 octahedral *z*-axis more closely into alignment with the crystallographic *b* axis. Realignment of the octahedra (which are related by a twofold axis) will tend to

bring octahedra 3 and 4 closer to 1 and 2, again leading to an overall contraction of the *c* axis.

In conclusion, we have shown in this paper that distortions of the ScO_6 and WO_4 polyhedra of $Sc_2(WO_4)_3$ as a function of temperature are relatively minor. The negative thermal expansion properties of this material can thus be viewed as being due to a complex three-dimensionally coupled twisting of relatively rigid framework polyhedra. The individual tilts are caused by the anharmonic nature of the transverse vibrations of the bridging oxygen atoms in the structure. These tilts lead to an effective decrease in the average Sc–O–W bridging bond angle as a function of temperature. This in turn leads to a decrease in the average metal–metal distance and is the main cause of the observed intrinsic negative thermal expansion of $Sc_2(WO_4)_3$.

ACKNOWLEDGMENTS

This work was supported by NSF Grant DMR-9308530. The neutron diffraction data were collected at the high flux beam reactor at Brookhaven National Laboratory, which is supported by the Division of Materials Sciences, U.S. Department of Energy, under contract DE-AC02-76CH0016l. The authors thank T. Vogt for assistance in collection of the neutron diffraction data.

REFERENCES

1. A. W. Sleight, *Endeavour* **19,** 64 (1995).
2. V. Korthuis, N. Khosrovani, A. W. Sleight, N. Roberts, R. Dupree, and W. W. Warren, Jr., *Chem. Mater.* **7,** 412 (1995).
3. N. Khosrovani, V. Korthius, and A. W. Sleight, *Inorg. Chem.* **35,** 485 (1996).
4. T. A. Mary, J. S. O. Evans, A. W. Sleight, and T. Vogt, *Science* **272,** 90 (1996).
5. J. S. O. Evans, T. A. Mary, T. Vogt, M. A. Subramanian, and A. W. Sleight, *Chem. Mater.* **8,** 2809 (1996).
6. J. S. O. Evans, T. A. Mary, and A. W. Sleight, *J. Solid State Chem.* **133,** 580 (1997).
7. J. S. O. Evans, T. A. Mary, and A. W. Sleight, *Physica B*, in press.
8. S. C. Abrahams and J. L. Bernstein, *J. Chem. Phys.* **45,** 2745 (1996).
9. T. Vogt,, L. Passell, S. Cheung, and J. D. Axe, *Nucl. Instrum. Methods Phys. Res., Sect. A* **338,** 71 (1993).
10. J. D. Axe, S. Cheung, D. E. Cox, L. Passell, and T. Vogt, *J. Neutron Res.* **2,** 85 (1994).
11. A. C. Larson and R. B. Von Dreele, LANSCE, Los Alamos National Lab, Los Alamos, NM, 1994.
12. J. D. Dunitz, V. Schomaker, and K. N. Trueblood, *J. Phys. Chem.* **92,** 856 (1988).
13. R. T. Downs, G. V. Gibbs, and M. B. Boisen, Jr., *Am. Miner.* **75,** 1253 (1990).
14. R. T. Downs, C. V. Gibbs, K. L. Bartelmehs, and M. B. Boisen, Jr., *Am. Miner.* **77,** 751 (1992).
15. S. Ghose, V. Schomaker, and R. K. McMullan, *Z. Kristallogr.* **176,** 159 (1986).
16. G. S. Pawley, *Acta Crystallogr.* **17,** 457 (1964).
17. G. S. Pawley, *Acta Crystallogr.* **20,** 631 (1966).
18. V. Schomaker and K. N. Trueblood, *Acta. Crystallogr. Sect. B* **24,** 63 (1968).
19. W. R. Busing and H. A. Levy, *Acta Crystallogr.* **17,** 142 (1964).
20. H. D. Megaw, "Crystal Structures: A Working Approach," Chap. 15. W. B. Saunders, New York, 1973.
21. D. W. Cruickshank, *Acta Crystallogr.* **9,** 757 (1956).
22. H. D. Megaw, *Z. Kristallogr. Sect. A* **100,** 58 (1938).
23. R. M. Hazen and C. T. Prewitt, *Amer. Miner.* **62,** 309 (1977).
24. G. W. Hallum and R. K. Datta, *J. Am. Ceram. Soc.* **68,** C68 (1985).
25. W. R. Buessem, *in* "Mechanical Properties of Engineering Ceramics," (W. W. Kreigel and H. Palmour III, Eds.), p. 127. Interscience, New York, 1961.
26. V. A. Balashov, G. I. Verona, A. A. Maier, and O. P. Proshina, *Izv. Akad. Nauk SSSR, Neorg. Mater.* **11,** 1713 (1975).
27. J. S. O. Evans, T. A. Mary, and A. W. Sleight, *J. Solid State Chem.* **120,** 101 (1995).